Simulation of a practical scramjet inlet using shock-unsteadiness model

Amjad Ali Pasha, C. Vadivelan, and Krishnendu Sinha

1 Introduction

The main function of a scramjet inlet is to capture air flow from the incoming hypersonic stream, compress it through a series of shocks or compression waves, and provide uniform flow to the combustor. There should be maximum mass capture along with a minimum stagnation pressure loss in the inlet.

The shock waves in the inlet duct interact with the boundary layer on the walls and can result in flow separation due to strong adverse pressure gradient across the shock wave. The shock/boundary-layer interaction often results in a complex flow pattern, comprising of additional shocks, expansion waves, shear layer and separation bubble. The separation bubbles are highly viscous, and hence increase the stagnation pressure loss. Peak values of pressure, skin friction and heat transfer rates are found at reattachment point. Also, the separation bubble acts as a blockage to the flow inside the inlet duct and can result in inlet unstart. It is therefore important to predict the shock/boundary-layer interactions in a scramjet inlet, including the size of the recirculation region, accurately.

Reynolds-averaged Navier-Stokes methods are commonly used in simulation of practical configurations of engineering interest. However, their accuracy is often limited in shock dominated flows, where conventional turbulence models developed for low-speed flows do not predict the underlying physics correctly. Several modifications have been proposed in literature [1], namely, compressibility correction, realizability constraint, rapid-distortion correction and length-scale correction. Their performance vary from one test case to another.

The flowfield in a shock/boundary-layer interaction is inherently unsteady. Sinha *et al.* [2] found that unsteady shock interaction with incoming turbulence fluctuations dampens the amplification of turbulent kinetic energy. A correction was added to standard one- and two-equation turbulence models to account for this damping

Department of Aerospace Engineering, Indian Institute of Technology Bombay, Mumbai-400076, India

effect. The resulting model predictions were found to match DNS data of turbulent kinetic energy amplification across a shock. The shock unsteadiness modification when applied to canonical compression corner [3] and oblique shock impingement flows [4] improved the prediction of flow separation point, and the resulting pressure and skin friction distribution.

In a practical inlet configuration, presence of geometric variations add to the overall complexity of the flowfield. In the absence of experimental data, CFD is often relied upon to predict and improve the performance of scramjet inlets. It is therefore essential to perform detailed CFD simulations of the flowfield inside an inlet duct. The focus of the current work is to study the reflection of the cowl shock and to predict the resulting separation bubble size accurately using the shock-unsteadiness model.

2 Simulation methodology

We solve two-dimensional Reynolds-averaged Navier-Stokes (RANS) equations. The Spalart-Allmaras (SA) turbulence model with shock-unsteadiness correction [3] is used in the simulations. In-house code [5] based on finite-volume formulation of the governing equations and a modified low-dissipation form of the Steger-Warming flux splitting approach is used. The discretization method is second-order accurate in space. The implicit Data Parallel Line Relaxation method is used to integrate the equations in time and reach a steady-state solution. The code has been validated for several supersonic and hypersonic flow applications [3, 4].

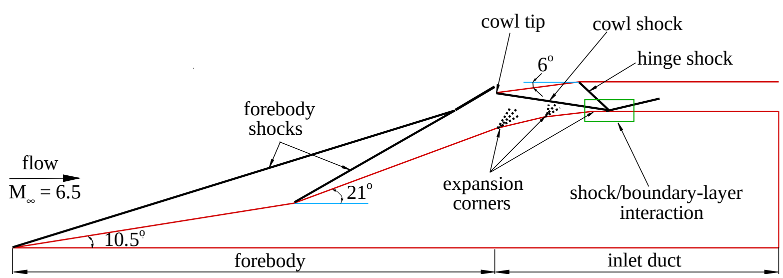

Fig. 1 Geometric configuration with flow schematic for the scramjet inlet.

A scramjet inlet of the mixed-compression type is shown in Fig. 1. The geometry consists of two forebody ramps of 10.5° and 21° respectively, followed by three expansion corners, each of 7°, leading to the inlet duct. The forebody shocks and expansion fans are shown in the figure.

The cowl is bent by 6° and results in formation of oblique shocks from the cowl tip and hinge location. The shock/boundary-layer interaction due to the impingement of the cowl and hinge shocks on the opposite wall is marked in the figure.

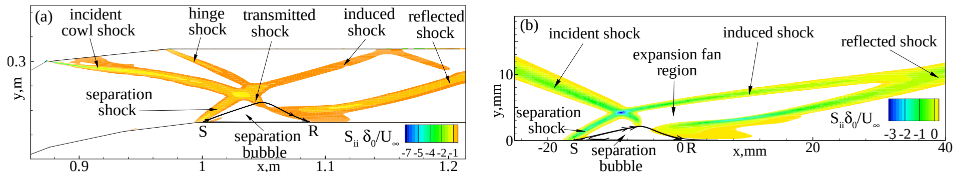

Fig. 2 Normalized dilatation contours identifying shock regions in (a) the inlet duct and (b) oblique shock/boundary-layer interaction with deflection angle of 14° at Mach 5.

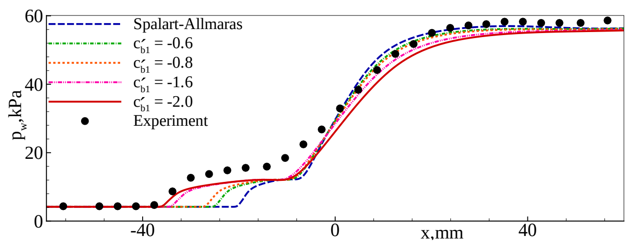

Fig. 3 Computed wall pressure using standard SA model [6] and shock-unsteadiness modified SA model [3] with deflection angle of 14° and $M_\infty = 5$, compared with experiments [7].

Freestream conditions of M_∞ = 6.5, temperature = 219.3 K and pressure = 2.16 kPa correspond to an altitude of 26 km. Isothermal ($T_w = 300$ K), no-slip and zero pressure gradient boundary conditions are assigned at solid boundaries. An extrapolation condition is specified

at the exit of the inlet duct. Freestream and wall conditions for turbulence model are calculated from the formulations used in Ref. [3].

Based on a separate grid refinement study, a 337×190 mesh is used for the simulation. A wall-normal spacing of 1×10^{-6} m corresponds to about 0.35 wall units on the forebody and less than 1.7 wall units in the inlet duct. CFL numbers up to 1000 are used in the simulation and it takes 40-cpu hours to obtain a steady state solution.

The computed shock-structure inside the inlet duct is shown in Fig. 2a in terms of the normalized mean dilatation contours. The shock structure is similar to that obtained in the interaction of an incident oblique shock with a flat plate boundary layer, shown in Fig. 2b. The incident shock, separation shock, induced shock, transmitted shock and reflected shock follow the same pattern in the two flows. The differences are the additional shock generated by the hinge and the reflection of the induced shock from the top wall. These are not present in the isolated shock impingement case shown in Fig. 2b.

The impingement of an incident oblique shock on a turbulent boundary layer developed on a flat-plate is studied experimentally in Ref. [7]. Measurements are taken in the shock/boundary-layer interaction region for 14° shock generator at Mach 5. The variation of surface pressure in the interaction region is plotted in Fig. 3 where the initial pressure rise at $x \approx -38$ mm represents the separation location. It is apparent that the standard SA model predicts a delayed separation ($x \approx -20$ mm) as compared to the experiment. The shock-unsteadiness correction reduces the turbulent eddy viscosity at the separation shock and thus enhances flow separation. Solutions computed using different values of the shock-unsteadiness parameter c'_{b_1} are also plotted in Fig. 3. A higher magnitude of c'_{b_1} yields a larger separation, and c'_{b_1} = -2.0 is found to match the experimental separation location closely. This value of the shock-unsteadiness parameter is found to match the separation location for a range of shock strengths and therefore it is used in the study of cowl shock impingement.

3 Flowfield and wall data

Figure 4 shows the flowfield in the inlet duct in terms of computed pressure contours. The cowl shock and hinge shock impinge on the turbulent boundary layer on the vehicle wall and form a recirculation region. A separation shock is formed at the separation point and a shear layer develops over the separation bubble. Intersection of the separation and incident shocks generate the induced and transmitted shock waves. The flow turns over the separation bubble to generate an expansion fan. The compression waves generated by flow reattachment coalesce to form the reflected shock. There are multiple reflections of shocks and expansion waves in the duct.

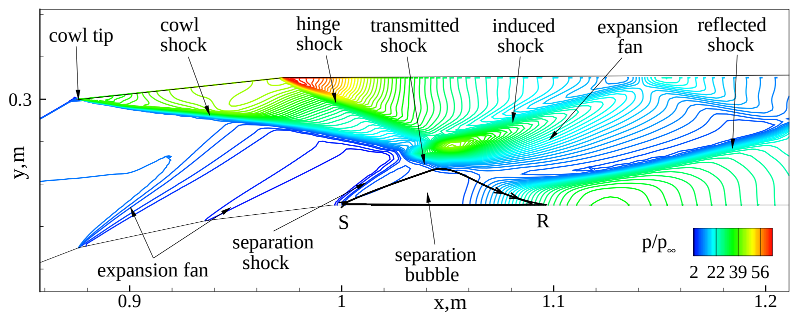

Fig. 4 Distribution of computed pressure, normalized by freestream pressure, inside the inlet duct.

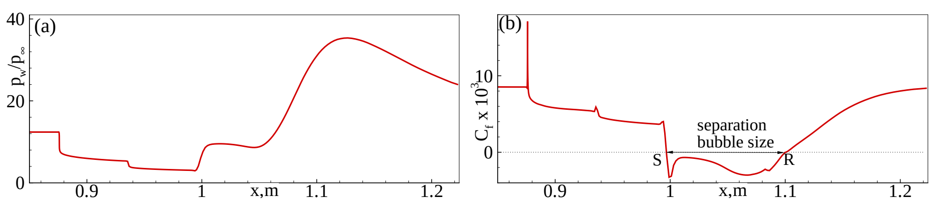

Fig. 5 Computed (a) normalized wall pressure and (b) skin-friction coefficient on the inlet duct bottom wall.

The surface pressure and skin-friction coefficient along the inlet bottom wall is shown in Fig. 5. The wall pressure drops across the two expansion corners at x = 0.86 m and x = 0.94 m. The expansion fan at the third expansion corner is cancelled by the separation shock. Pressure rises at flow separation, remains approximately constant along the separation bubble and rises to peak values in the reattachment region. The skin friction data shows a large negative region between the separation (S) and reattachment (R) points. The separation bubble is 104 mm long in the streamwise direction and extends to about one third of the duct height.

The computed separation bubble size is compared with available experimental data to ascertain the accuracy of the results. In the absence of experimental data for the current geometry, the data reported by Schulein [7] is used for validation. Specifically, the size of the separation bubble predicted in the inlet duct is compared with those reported in the oblique shock impingement experiments. The variations due to differences in the inflow conditions are accounted for three cases reported in Ref. [7], which correspond to shock generator angles of 14°, 10° and 6° placed in a Mach 5 flow. By comparison, the flow conditions at the entrance of the inlet duct correspond to a Mach number of 3.4, density of 0.089 kg/m^3 and temperature of 382.2 K. These are the inviscid conditions downstream of the forebody ramp shock.

Parameters	Inlet	Oblique shock impingement		
		case-1	case-2	case-3
Free stream Mach number, M_∞	3.4	5	5	5
Deflection angle, θ°	15	14	10	6
Inviscid incident shock strength, p_2/p_1	11.34	13.62	7.63	3.76
Unit Reynolds number, $Re_{1\infty} \times 10^7$, m^{-1}	0.74	3.7	3.7	3.7
Upstream boundary layer thickness, δ_0, mm	22.7	4.66	4.66	4.66
Separation bubble size, Δs, mm	104	34	12	-
Normalized separation bubble size, $\Delta s/\delta_0$	4.58	7.30	2.58	-

Table 1 Comparison of flow parameters between the scramjet inlet configuration and oblique shock impingement cases [7].

The extent of flow separation in a shock/boundary-layer interaction mainly depends on the shock strength and the Reynolds number of the flow. A stronger incident shock wave results in a larger separation bubble and vice versa. On the other hand, a higher Reynolds number results in a higher level of turbulence. This in turn leads to a fuller boundary layer profile, thus resulting in delay of flow separation. Also, the separation bubble size is found to scale with the boundary layer thickness upstream of the interaction. These parameters are listed for the current configuration and for the three test cases of Schulein [7] in Table 1.

Deflection of a Mach 3.4 flow by the cowl shock results in a pressure rise of 11.34. A comparison of the inviscid pressure rise values places the shock/boundary-layer interaction in the inlet duct between the experimental test cases 1 and 2. The recirculation bubble in the inlet duct is however much larger than those reported in the experiments. This is because of a thicker boundary layer than that in the experimental cases. On normalizing the separation bubble size with the incoming boundary layer thickness, the simulation results compare well with the experimental data. From above analysis, $\Delta s/\delta_0 = 4.58$ for the inlet duct lies in between the experimental test cases 1 and 2.

4 Conclusions

Reynolds-averaged Navier-Stokes simulations are performed for a practical scramjet inlet geometry at Mach 6.5 and the focus is the shock/boundary-layer interaction generated by cowl shock impingement on the opposite wall. The flow is similar to the canonical oblique shock/boundary-layer interaction. The geometry of the inlet generates additional shocks and expansion waves and adds to the complexity to the flowfield. The shock-unsteadiness modified Spalart-Allmaras model is used in the simulations and the model parameter is calibrated against experimental data for canonical oblique shock/boundary-layer interactions. The simulations predict a large separation bubble inside duct and its size is validated against available experimental data for canonical flow configurations.

Acknowledgment

The authors thank Indian Space Research Organization (ISRO) for supporting this research under the RESPOND programme.

References

1. Roy, C. J., and Blottner, F. G. "Review and Assessment of Turbulent Models for Hypersonic Flows," *Progress in Aerospace Sciences*, Vol. 42, No. 7-8, 2006, pp. 469-530.
2. Sinha, K., Mahesh, K., and Candler, G. V. "Modeling Shock Unsteadiness in Shock/Turbulence Interaction", *Physics of Fluids*, Vol.15, No.8, 2003, pp. 2290-2297.
3. Sinha, K., Mahesh, K., and Candler, G. V. "Modeling the Effect of Shock-Unsteadiness in Shock/Turbulent Boundary-Layer Interactions", *AIAA Journal*, Vol.43, No.3, pp.586-594, 2005.
4. Pasha, A. A., and Sinha, K. "Shock-Unsteadiness Model Applied to Oblique Shock-Wave/Turbulent Boundary-Layer Interaction," *International Journal of Computational Fluid Dynamics*, Vol. 22, No. 8, 2008, pp. 569-582.
5. Sinha, K., and Candler, G. V. "Convergence Improvement of Two-Equation Turbulence Model Calculations", *AIAA Paper*, 98-2649, June 1998.
6. Spalart, P. R., and Allmaras, S. R. "A One-equation Turbulence Model for Aerodynamic Flows," *AIAA Paper*, AIAA-92-0439, Reno, NV, Jan. 1992.
7. Schulein, E. "Optical Skin Friction Measurements in Short-duration Facilities", *AIAA Journal*, Vol. 44, No.8, 2006, pp.1732-1742.